

Article

Optimization and Comparison of Two Combined Cycles Consisting of CO₂ and Organic Trans-Critical Cycle for Waste Heat Recovery

Liya Ren  and Huaixin Wang *

MOE Key Laboratory of Efficient Utilization of Low and Medium Grade Energy, School of Mechanical Engineering, Tianjin University, Tianjin 300072, China; renly@tju.edu.cn

* Correspondence: wanghx@tju.edu.cn

Received: 3 January 2020; Accepted: 4 February 2020; Published: 7 February 2020



Abstract: CO₂-based trans-critical and supercritical cycles have received more and more attention for power generation in many applications such as solar and nuclear energy due to the desirable thermal stability and properties of CO₂ and the high efficiency and compact size of the plant. In this study, two combined cycles driven by the flue gas exhausted from the LM2500+ gas turbine, CO₂-TC+OTC (organic trans-critical cycle) and CO₂-TC/OTC, which can achieve a good trade-off between thermal efficiency and utilization of the waste heat, are investigated. Parameters optimization is carried out by means of genetic algorithm to maximize the net power output of the combined cycle and the effects of the key parameters on the cycle performance are examined. Results show that the exergy efficiency of CO₂-TC+OTC is about 2% higher than that of CO₂-TC/OTC. In CO₂-TC+OTC, the recuperation process of CO₂ causes the largest exergy loss; in CO₂-TC/OTC, the largest exergy loss occurs in the heat recovery vapor generator, followed by the intermediate heat exchanger due to the larger variation of the specific heat capacity of CO₂ and organic fluid in the heat addition process.

Keywords: CO₂ trans-critical cycle; organic trans-critical cycle; combined cycle; waste heat recovery; thermodynamic optimization

1. Introduction

Recovering waste heat from the engines, gas turbines and industrial processes such as cement, glass and metallurgy and so forth, can effectively improve energy utilization efficiency, thus reducing fossil fuel consumption and CO₂ emissions. In addition to the direct heat utilization of waste heat, such as preheating air and raw materials, building heating and so forth, power recovery is another practical option, especially for the medium-to-high temperature waste heat sources.

Organic Rankine cycle (ORC) and organic trans-critical cycle (OTC) prove to be the promising technologies for the heat to power conversion under the low-to-medium temperature heat sources [1], which is mainly attributed to the lower critical temperature and the dry or isentropic characteristics of the organic working fluids. However, the organic compounds will suffer thermal decomposition at relatively high temperature, which affects the performance of ORC and OTC under the medium-to-high heat source conditions. Thus, carbon dioxide (CO₂) has attracted more and more attention due to its high thermal stability. Additionally, it is environmentally friendly, non-corrosive, non-toxic, non-flammable, easy to obtain and with the desirable heat and mass transfer properties.

As the critical temperature of CO₂ is relatively low (30.98 °C), trans-critical cycle (TC) and supercritical cycle (SC) with CO₂ as the working fluid are commonly considered for the waste heat recovery. The CO₂-TC features that the pressure of the heat addition process is higher than the critical pressure of CO₂, while the heat rejection pressure is lower than the critical pressure. Both the pressures

of heat addition and heat rejection process of CO₂-SC are above the critical pressure of CO₂. Unlike the general Brayton cycle, the CO₂ at the compressor inlet of CO₂-SC is near the critical point, which is mainly to reduce the power consumption of the compression process since CO₂ behaves more like an incompressible fluid in this region. A better temperature match between the flue gas and the supercritical CO₂ can be achieved in the CO₂-TC and CO₂-SC, which enables the smaller exergy loss in the heat addition process of CO₂ and higher utilization efficiency of the waste heat. In addition, the higher fluid density of supercritical CO₂ and the lower volume ratio in the expansion process permits the efficient and compact turbomachinery design.

The critical pressure of CO₂ is 7.38 MPa. Considering the conventional cooling water condition, the heat rejection pressure of CO₂-TC is just slightly lower than the critical pressure [2]. Therefore, the pressure ratio of CO₂-TC and CO₂-SC is limited since the high pressure may threaten the safety of the system. The lower pressure ratio results in a lower temperature drop during the expansion process, which is detrimental to the thermal efficiency of the cycle. In this context, introducing a recuperator to recover the heat of turbine exhaust is an efficient solution to improve the cycle thermal efficiency. Echogen Power System LLC has developed the waste heat power system scalable from 250 kW to greater than 50 MW using the CO₂-SC technology and they proved that the recuperative CO₂-SC can provide the higher power output with the lower levelized cost of energy (LCOE) than the conventional steam Rankine cycle for the waste heat recovery of gas turbine [3].

In a recuperator, the cold side is the high pressure supercritical fluid and the hot side is the low-pressure vapor (for CO₂-TC) or supercritical fluid (for CO₂-SC). The specific heat capacity of the CO₂ on both sides is quite different, especially in the low-temperature region (see Figure 1a), which leads to the lower recuperator effectiveness and larger exergy loss in the heat transfer process, as the T-Q diagram shows in Figure 1b. To compensate the drawback, the recompressed recuperative cycle is proposed, in which the recuperation process is occurred in two heat exchangers-high temperature recuperator and low temperature recuperator. The temperature match can be improved by adjusting the mass flow ratio of the cold and hot fluid in the low-temperature recuperator. Thus, the recompressed recuperative cycle shows the highest thermal efficiency among different cycle configurations based on CO₂-SC [4].

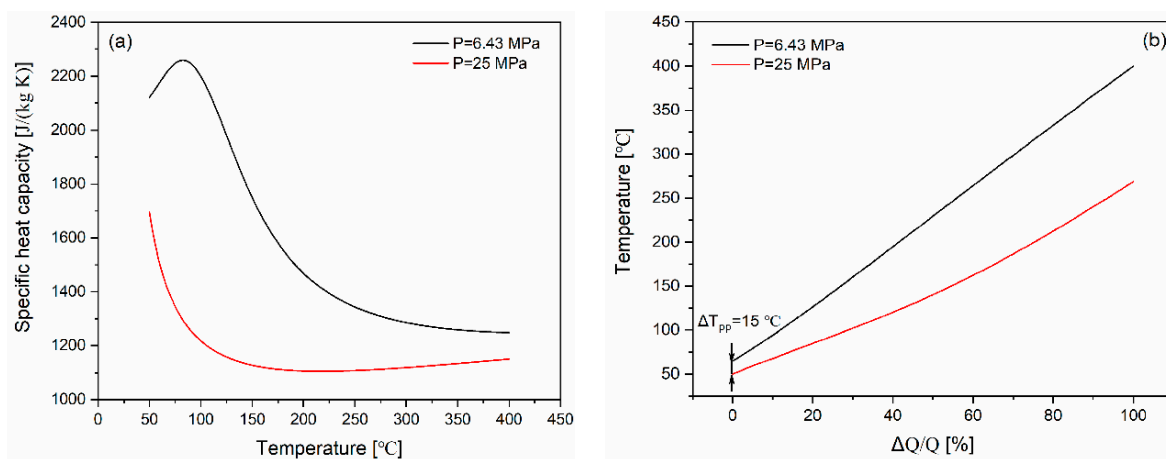


Figure 1. The (a) specific heat capacity and (b) temperature match of the two sides in the recuperator of CO₂-TC.

In some applications, the higher thermal efficiency is the design objective for the CO₂-TC and CO₂-SC, such as nuclear [5], coal-fired [6] and solar [7] power plants. However, when it comes to waste heat recovery, we pay more attention to maximizing the net power output of the system since the waste heat is generally discharged into the environment after releasing heat to the plant. The recuperation and recompression mentioned above can increase the heat absorption temperature of CO₂, which will accordingly reduce the heat extraction from the waste heat source.

To achieve the deep utilization of the waste heat for CO₂-TC and CO₂-SC systems, integrating a bottom cycle X to absorb the residual heat of the heat source is an effective solution, forming the CO₂-TC(SC)+X combined cycle. The proposed bottom cycles include CO₂-SC [8], CO₂-TC [9] and ORC [10]. Another solution to ensure the higher utilization efficiency of the waste heat is to use a bottom cycle Y to recover the heat of turbine exhaust CO₂ instead of using the recuperator, forming the CO₂-TC(SC)/Y combined cycle. Similarly, the bottom cycles can be CO₂-TC [11], CO₂-SC [12], ORC [13], OTC [14]. These researches have indicated that the two kinds of the combined cycle can achieve better thermodynamic performance than the stand-alone recuperated and recompressed CO₂-TC and CO₂-SC. It is worth mentioning that if the bottom cycle is the same as the top cycle, they can share some components, such as the cooler and compressor (for CO₂-SC) or condenser and pump (for CO₂-TC), so as to reduce the cost and space of the combined system. Correspondingly, the endothermic pressure and exothermic pressure of the top and bottom cycles must be kept equal respectively, which may lead to the insufficient optimization of the system performance.

Reference [15] gave a thorough literature review and detailed analysis of different layouts of CO₂-SC. However, the research of a clear comparison between the above two kinds of the combined cycle is quite rare. In this study, CO₂-TC is selected as the top cycle and OTC is selected as the bottom cycle owing to its better temperature match with the waste heat source, forming two combined cycles: CO₂-TC+OTC, CO₂-TC/OTC. The purpose of this study is to find out which of the two combined cycles shows better thermodynamic performance for waste heat recovery. The influence of some key parameters on the system performance is also examined. The parametric optimization is performed to maximize the net power output of the two combined cycles by using genetic algorithm based on the MATLAB platform and the control parameters in genetic algorithm (GA) have been described in our previous work [16]. Pentane and R134a are selected as the working fluid for OTC and the thermodynamic properties of the fluids are calculated by the Refprop NIST 9.0 [17]. The waste heat source to drive the combined cycles is from the LM2500+ gas turbine [18] and the initial temperature and mass flow rate of the exhaust gas are 533.8 °C and 89.5 kg/s.

2. System Descriptions

2.1. CO₂-TC+OTC

According to the results of Reference [10], the thermodynamic and economic performance of the combined cycle CO₂-SC+ORC with regenerative CO₂-SC as the top cycle is superior to that with recompressed CO₂-SC. Hence, a single recuperated layout of CO₂-TC is considered in this study.

The schematic and T-s diagrams of the regenerative CO₂-TC+OTC combined system are shown in Figures 2 and 3. The exhaust gas releases heat to the CO₂ and organic fluid in HRVG1 and HRVG2 (heat recovery vapor generator) successively. The generated high temperature CO₂ and organic fluid expand in the turbine1 and turbine2 to do work (1H–2H, 1L–2L) respectively. The organic fluid exhausted from turbine2 flows into the condenser2 and releases heat to the cooling water (2L–4L). The saturated liquid leaving the condenser2 will be pressurized by the pump2 (4L–5L) and then enters the HRVG2 to absorb heat from the heat source (5L–1L). The exhaust CO₂ from turbine1 enters the recuperator to preheat the low-temperature CO₂ coming from the pump1 (2H–3H) and then liquefied by the cooling water in the condenser1 (3H–4H). The liquid CO₂ exiting condenser1 is compressed by the pump1 (4H–5H) and heated in the recuperator (5H–6H) before flowing into the HRVG1 to absorb the waste heat (6H–1H).

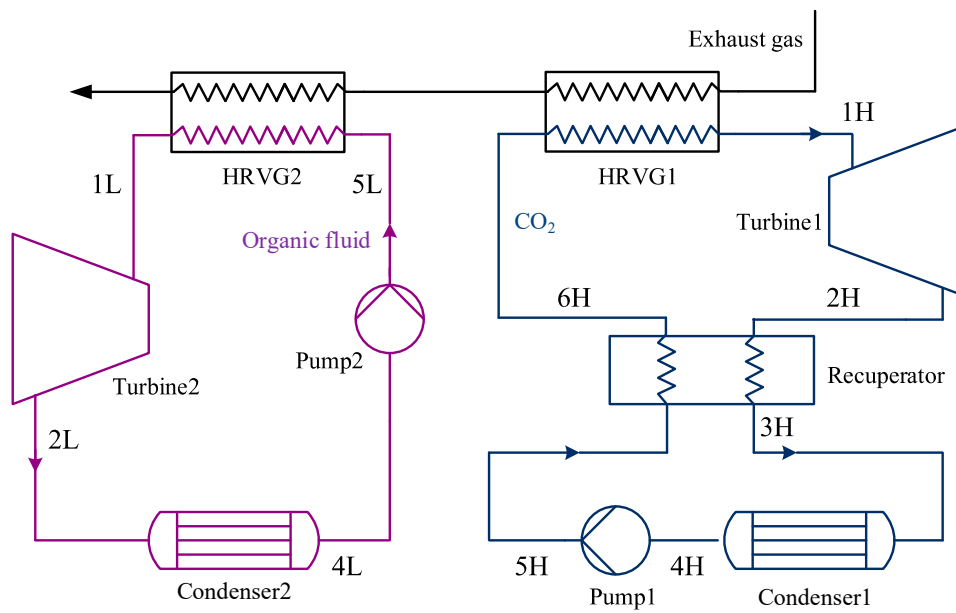


Figure 2. Schematic diagram of CO₂-TC+OTC combined system.

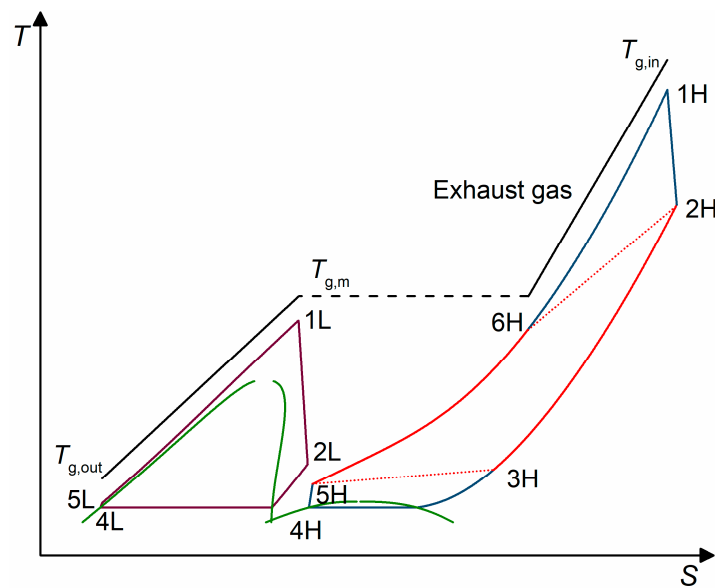


Figure 3. T-s diagram of CO₂-TC+OTC combined system.

2.2. CO₂-TC/OTC

The schematic and T-s diagrams of the CO₂-TC/OTC combined system are shown in Figures 4 and 5. To extract as much heat as possible from the waste heat source, the recuperator is not included in the top CO₂-TC, which means the CO₂ stream at pump1 exit flows directly into the HRVG without preheating. The CO₂ stream exhausted from turbine1 drives the bottom OTC system and the organic fluid is heated in the IHE (intermediate heat exchanger).

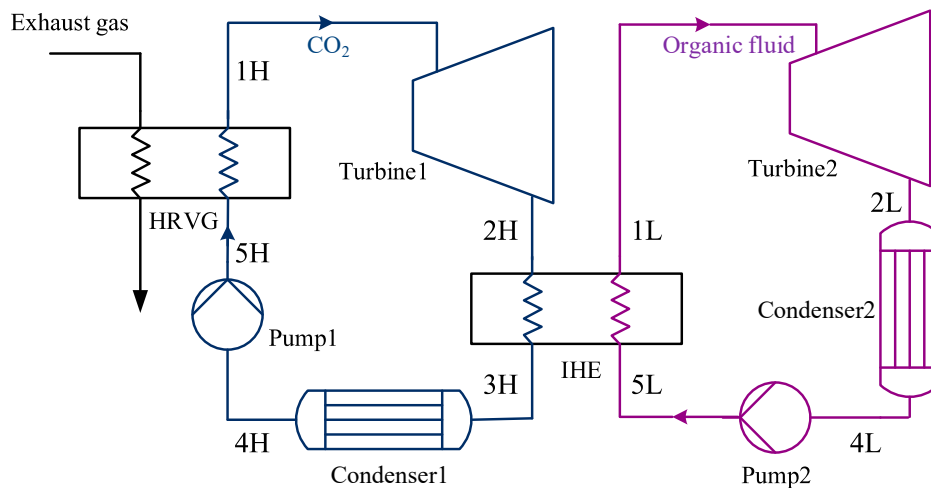


Figure 4. Schematic diagram of CO₂-TC/OTC combined system.

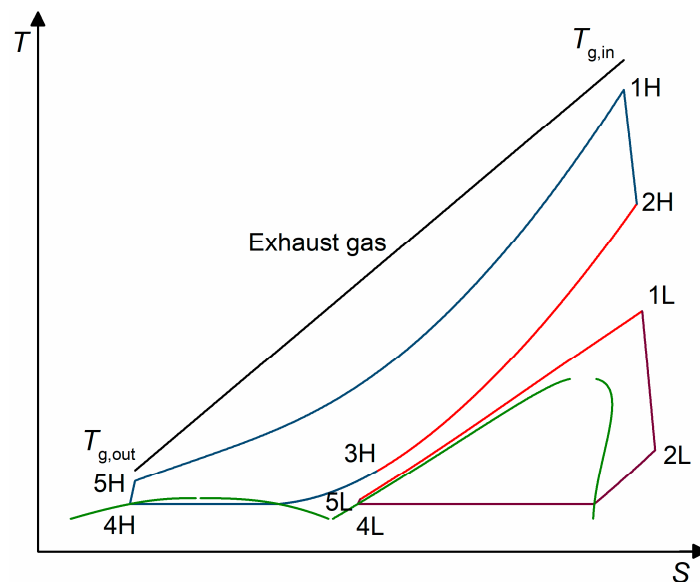


Figure 5. T-s diagram of CO₂-TC/OTC combined system.

3. Methodology

3.1. Thermodynamic Modeling

The following assumptions were made in establishing the thermodynamic models of the combined system. The working fluid was in a steady flow state in each component. The change in kinetic and potential energies of working fluid flowing in the system was negligible. The pressure drop and heat dissipation in the heat exchangers and pipes were also neglected.

Table 1 gives the energy and exergy balance equations in each component of the two combined cycles. Wherein, \dot{Q} is the heat transferred in the process, kW; \dot{m} , h and s denote the mass flow rate, enthalpy and entropy of the fluid, kg/s, kJ/kg, kJ/(kgK); T_0 means the ambient temperature, K; \dot{W} refers to the power input or output of the process, kW; I is the exergy loss of the process, kW. The equations in turbine1, condenser1, pump1, turbine2, condenser2, pump2 of CO₂-TC/OTC are the same as that of the CO₂-TC+OTC.

Table 1. Thermodynamic models in each component of the two combined cycles.

Component	Equations
CO₂-TC+OTC	
HRVG1	$\dot{Q} = \dot{m}_g(h_{g,in} - h_{g,m}) = \dot{m}_{wf,CO_2}(h_{1H} - h_{6H})$ $\dot{I} = T_0[\dot{m}_{wf,CO_2}(s_{1H} - s_{6H}) - \dot{m}_g(s_{g,in} - s_{g,m})]$
Turbine1	$\dot{W}_{turb,1} = \dot{m}_{wf,CO_2}(h_{1H} - h_{2H}) = \dot{m}_{wf,CO_2}(h_{1H} - h_{2Hs})\eta_{turb,CO_2}$ $\dot{I} = T_0\dot{m}_{wf,CO_2}(s_{2H} - s_{1H})$
Recuperator	$\dot{Q} = \dot{m}_{wf,CO_2}(h_{2H} - h_{3H}) = \dot{m}_{wf,CO_2}(h_{6H} - h_{5H})$ $\dot{I} = \dot{m}_{wf,CO_2}T_0[(s_{6H} - s_{5H}) - (s_{2H} - s_{3H})]$
Condenser1	$\dot{Q} = \dot{m}_{wf,CO_2}(h_{3H} - h_{4H})$ $\dot{I} = \dot{m}_{wf,CO_2}[h_{3H} - h_{4H} - T_0(s_{3H} - s_{4H})]$
Pump1	$\dot{W}_{pump,1} = \dot{m}_{wf,CO_2}(h_{5H} - h_{4H}) = \dot{m}_{wf,CO_2}(h_{5Hs} - h_{4H})/\eta_{pump}$ $\dot{I} = T_0\dot{m}_{wf,CO_2}(s_{5H} - s_{4H})$
HRVG2	$\dot{Q} = \dot{m}_g(h_{g,m} - h_{g,out}) = \dot{m}_{wf,organic}(h_{1L} - h_{5L})$ $\dot{I} = T_0[\dot{m}_{wf,organic}(s_{1L} - s_{5L}) - \dot{m}_g(s_{g,m} - s_{g,out})]$
Turbine2	$\dot{W}_{turb,2} = \dot{m}_{wf,organic}(h_{1L} - h_{2L}) = \dot{m}_{wf,organic}(h_{1L} - h_{2Ls})\eta_{turb,organic}$ $\dot{I} = T_0\dot{m}_{wf,organic}(s_{2L} - s_{1L})$
Condenser2	$\dot{Q} = \dot{m}_{wf,organic}(h_{2L} - h_{4L})$ $\dot{I} = \dot{m}_{wf,organic}[h_{2L} - h_{4L} - T_0(s_{2L} - s_{4L})]$
Pump2	$\dot{W}_{pump,2} = \dot{m}_{wf,organic}(h_{5L} - h_{4L}) = \dot{m}_{wf,organic}(h_{5Ls} - h_{4L})/\eta_{pump}$ $\dot{I} = T_0\dot{m}_{wf,organic}(s_{5L} - s_{4L})$
CO₂-TC/OTC	
HRVG	$\dot{Q} = \dot{m}_g(h_{g,in} - h_{g,out}) = \dot{m}_{wf,CO_2}(h_{1H} - h_{5H})$ $\dot{I} = T_0[\dot{m}_{wf,CO_2}(s_{1H} - s_{5H}) - \dot{m}_g(s_{g,in} - s_{g,m})]$
IHE	$\dot{Q} = \dot{m}_{wf,CO_2}(h_{2H} - h_{3H}) = \dot{m}_{wf,organic}(h_{1L} - h_{5L})$ $\dot{I} = T_0[\dot{m}_{wf,organic}(s_{1L} - s_{5L}) - \dot{m}_{wf,CO_2}(s_{2H} - s_{3H})]$

The net power output of the combined cycle is given by:

$$\dot{W}_{net} = \dot{W}_{turb,1} + \dot{W}_{turb,2} - \dot{W}_{pump,1} - \dot{W}_{pump,2}. \quad (1)$$

The exergy efficiency of the combined cycle is defined as:

$$\eta_{ex} = \frac{\dot{W}_{net}}{\dot{m}_g[h_{g,in} - h_{g,0} - T_0(s_{g,in} - s_{g,0})]}, \quad (2)$$

where $h_{g,0}$ and $s_{g,0}$ are the enthalpy and entropy of exhaust gas when it is cooled to the ambient temperature.

3.2. Turbine Efficiency Calculation

A three-stage axial turbine was considered for the CO₂-TC and OTC systems. The turbine efficiency varies with the operating parameters and thermophysical properties of the working fluid. Reference [19] indicated that the turbine efficiency can be evaluated based on three independent variables including the size parameter SP , volume ratio Vr and the specific speed Ns . The calculation correlation for the maximum efficiency of a three-stage axial turbine under the optimum specific speed

given in Reference [19] is shown as Equation (3) and the coefficients used in the correlation are listed in Table 2.

$$\eta_{\text{turb}} = \sum_{i=0}^{12} A_i F_i. \quad (3)$$

Table 2. Coefficients used in the turbine efficiency calculation correlation [19].

n	F_i	A_i	n	F_i	A_i
0	1	0.932,274	7	$\ln(V_r)^4$	0.000,298
1	$\ln(\text{SP})$	-0.01,243	8	$\ln(V_r) \ln(\text{SP})$	0.005,959
2	$\ln(\text{SP})^2$	-0.018	9	$\ln(V_r)^2 \ln(\text{SP})$	-0.00,163
3	$\ln(\text{SP})^3$	-0.00,716	10	$\ln(V_r) \ln(\text{SP})^2$	0.001,946
4	$\ln(\text{SP})^4$	-0.00,118	11	$\ln(V_r)^3 \ln(\text{SP})$	0.000,163
5	V_r	-0.00,044	12	$\ln(V_r)^2 \ln(\text{SP})^3$	0.000,211
6	$\ln(V_r)^3$	-0.0016			

3.3. Decision Variables and Specified Parameters

The decision variables in the optimization process of the combined cycle were the turbine inlet pressure and temperature for CO₂-TC and OTC. The ranges of the variables are shown in Table 3. To ensure the safe and stable operation of the system, the maximum heat addition pressure of CO₂ and organic fluid as set as 25 MPa. In order to avoid liquid erosion of the turbine blades, the expansion process was not allowed to go through the saturated zone for the OTC system. $T_{\text{stable,limit}}$ refers to the maximum temperature at which the organic fluid does not decompose and the values of $T_{\text{stable,limit}}$ for pentane and R134a are 280 °C [20] and 368 °C [21] respectively.

Table 3. Decision variables and the lower and upper boundaries.

Decision Variables	Lower Limit	Upper Limit
CO₂-TC		
Turbine inlet pressure, P_{1H}	10 MPa	25 MPa
Turbine inlet temperature, T_{1H}	$T_{g,in} - 100$	$T_{g,in} - \Delta T_{pp}$
OTC		
Turbine inlet pressure, P_{1L}	$1.1P_{\text{crit}}$	25 MPa
Turbine inlet temperature, T_{1L}	$T_{\text{crit}} + 20$	$\min\{T_{g,m} - \Delta T_{pp}, T_{\text{stable, limit}}\}$ for CO ₂ -TC+OTC $\min\{T_{2H} - \Delta T_{pp}, T_{\text{stable, limit}}\}$ for CO ₂ -TC/OTC

The specified parameters of the combined system are listed in Table 4. The composition and mass fraction of the exhaust gas were as follows: N₂ = 76%, H₂O = 11%, CO₂ = 13%. The condensing temperature of both the CO₂-TC and OTC was 25 °C. It should be noted that the pinch point temperature difference always occurs at the outlet of hot fluid in the recuperator (see Figure 1b); however, in the heat exchange process between the exhaust gas and CO₂, the exhaust gas and organic fluid in HRVG, as well as between the CO₂ and organic fluid in IHE, the position of the pinch point temperature difference varies with the temperature and pressure of the fluids. Therefore, in the optimization process, the outlet temperatures of the hot fluid that is, $T_{g,m}$, $T_{g,out}$ and T_{3H} were instantaneously adjusted to ensure that the pinch point temperature difference in the heat exchange process was 15 °C.

Table 4. Specified parameters of the combined system.

Parameters	Value
Exhaust gas initial temperature, $T_{g,in}$	533.8 °C
Exhaust gas mass flow rate, \dot{m}_g	89.5 kg/s
Exhaust gas pressure, P_g	101.325 kPa
Ambient temperature, T_0	20 °C
Condensing temperature, T_{4L}, T_{4H}	25 °C
Pinch point temperature difference in HRVG, recuperator and IHE, ΔT_{pp}	15 °C
Working fluid pump efficiency, η_{pump}	0.8

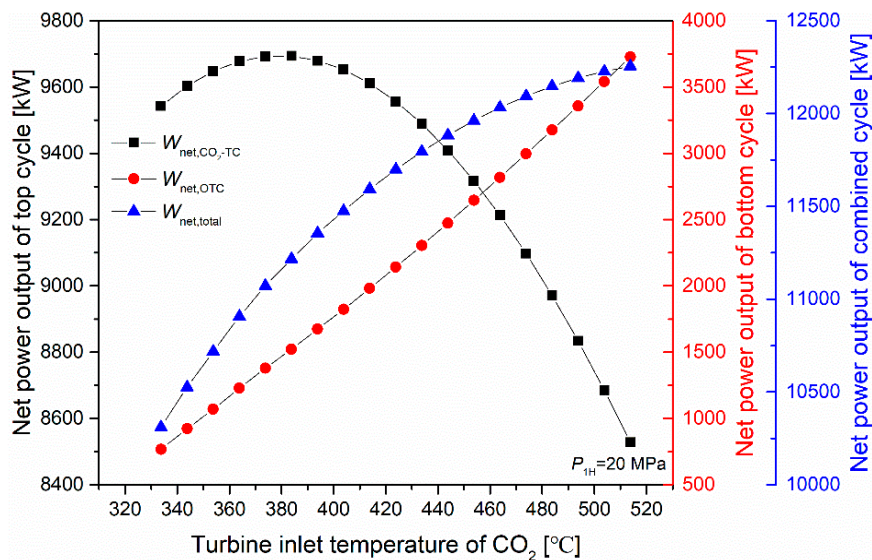
4. Results and Discussion

4.1. Performance Analysis of CO₂-TC+OTC

The variations of the net power output of CO₂-TC, OTC using R134a and combined cycle with the turbine inlet temperature of CO₂ (T_{1H}) are shown in Figure 6. The heat addition pressure of CO₂ (P_{1H}) remains at 20 MPa and the temperature of exhaust CO₂ (T_{2H}) increases with the increase of T_{1H} . After the recuperation process, the HRVG inlet temperature of CO₂ (T_{6H}) will rise accordingly, which results in the increase of thermal efficiency and the decrease of heat absorption of CO₂-TC. Hence, under the combined effect of the two trends, the net power output of CO₂-TC increases first and then decreases.

As the $T_{g,m}$ increases, the thermal efficiency and net power output of OTC increase. It should be noted that the net power output of OTC shown in Figure 6 is the maximum power under the heat source condition whose initial temperature is $T_{g,m}$ corresponding to different T_{1H} . The effects of turbine inlet temperature and pressure of the organic working fluid on the thermal efficiency and net power output of OTC have been illustrated in our previous work [16].

The increment of the net power output of OTC is greater than the decrement of the net power output of CO₂-TC. Thus, the maximum total net power output of the combined cycle is achieved when the T_{1H} reaches its upper limit.

**Figure 6.** Variations of net power output with turbine inlet temperature of CO₂ for CO₂-TC+OTC.

The variations of net power output with the turbine inlet pressure of CO₂ (P_{1H}) are shown in Figure 7. The T_{1H} is kept at the upper limit of 518.8 °C. The thermal efficiency and heat addition of CO₂-TC increase with the increase of P_{1H} , which leads to an increase in the net power output of CO₂-TC. The net power output of OTC decreases as the $T_{g,m}$ decreases, while its decrement is lower than the increment of the net power output of CO₂-TC. Thus, the optimum P_{1H} to maximize the net power output of the combined cycle is 25 MPa.

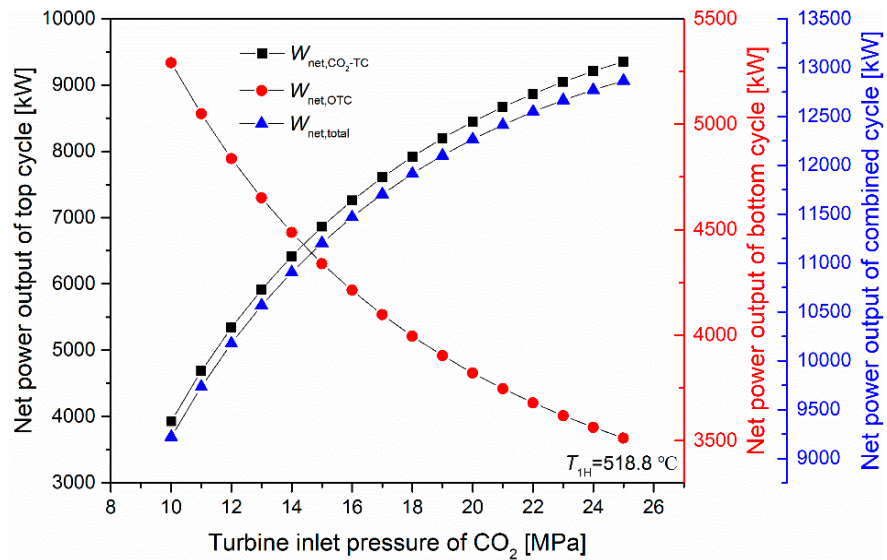


Figure 7. Variations of net power output with turbine inlet pressure of CO₂ for CO₂-TC+OTC.

The decision variables of the combined cycle CO₂-TC+OTC with R134a and pentane as the working fluid are optimized by using genetic algorithm. The variations of the net power output of the combined cycle with generation in the optimization process are shown in Figure 8. It can be seen that when the generation reaches about 50, the result tends to converge.

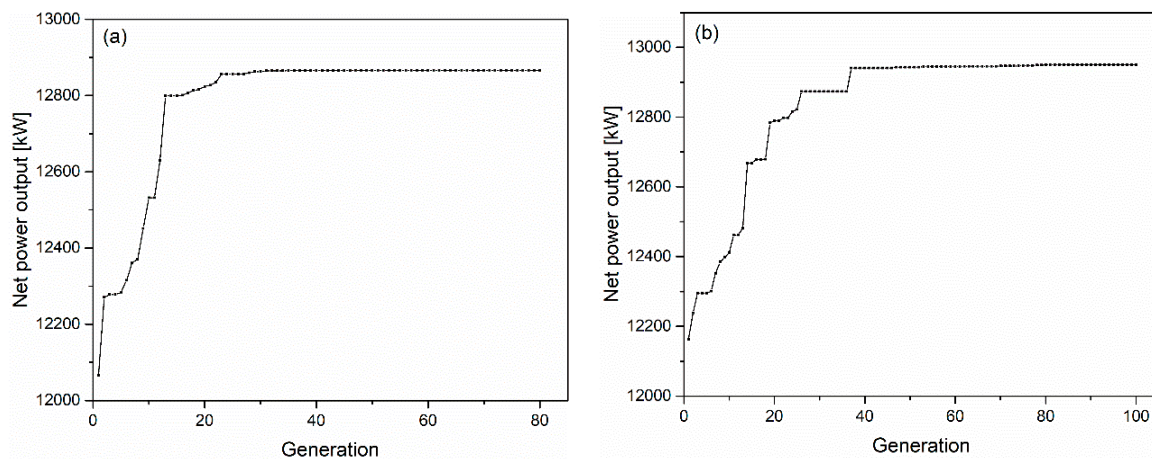


Figure 8. Variation of objective function value with generation for CO₂-TC+OTC (a) R134a, (b) Pentane.

The optimized variables and the maximum net power output of the combined cycle CO₂-TC+OTC are listed in Table 5. As analyzed above, the optimal turbine inlet temperature and pressure of CO₂ are their respective upper limits. The net power output of the bottom cycle OTC is approximately 40% of that of the top cycle CO₂-TC and OTC using pentane achieves a slightly higher net power output than that using R134a. Figure 9 reveals the T-Q diagram of the exhaust gas and working fluid and it can be seen that the thermal matching better the heat source and working fluid is quite better for the CO₂-TC+OTC combined cycle.

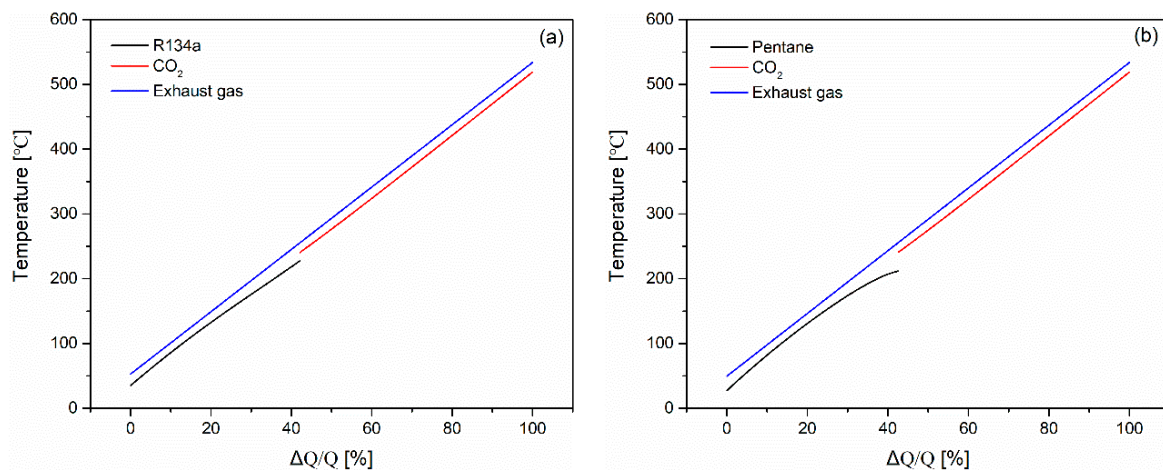


Figure 9. T-Q diagram of exhaust gas and working fluid for CO₂-TC+OTC (a) R134a, (b) Pentane.

Table 5. Optimized variables and cycle performance of two combined cycles.

Working Fluid	P_{1H} (MPa)	T_{1H} (°C)	P_{1L} (MPa)	T_{1L} (°C)	$T_{g,out}$ (°C)	$\dot{W}_{net,OTC}$ (kW)	\dot{W}_{net,CO_2-TC} (kW)	$\dot{W}_{net,total}$ (kW)
CO₂-TC+OTC								
Pentane	25	518.8	4.3	211.8	49.4	3601.2	9353.9	12,955.1
R134a	25	518.8	16.6	227.6	52.7	3511.4	9353.9	12,865.3
CO₂-TC/OTC								
Pentane	25	518.8	4.47	230.9	70.2	4607.8	7966.6	12,574.4
R134a	25	518.8	25	305.7	70.2	4523.3	7966.6	12,489.9

4.2. Performance Analysis of CO₂-TC/OTC

Figure 10 indicates the variations of the outlet temperature of the pump (T_{5H}) and turbine (T_{2H}) and thermal efficiency with the heat addition pressure of CO₂ (P_{1H}) for the top cycle CO₂-TC. The higher P_{1H} results in the higher T_{5H} and the lower T_{2H} . The former leads to the increase of exhaust gas outlet temperature, which means the reduction of heat release for the heat source, while the latter increases the cycle thermal efficiency. The detrimental effect of the heat absorption reduction on the net power output of the cycle is less than that of the beneficial effect of the thermal efficiency increase. Thus, the net power output of CO₂-TC increases as the P_{1H} increases, as shown in Figure 11. The maximum net power output of OTC with R134a as the working fluid will decrease with the decrease of T_{2H} , yet its decrement is smaller than the net power output increment of CO₂-TC. Hence, as illustrated in Figure 11, increasing the heat addition pressure of CO₂ helps to increase the total net power output of the combined cycle CO₂-TC/OTC.

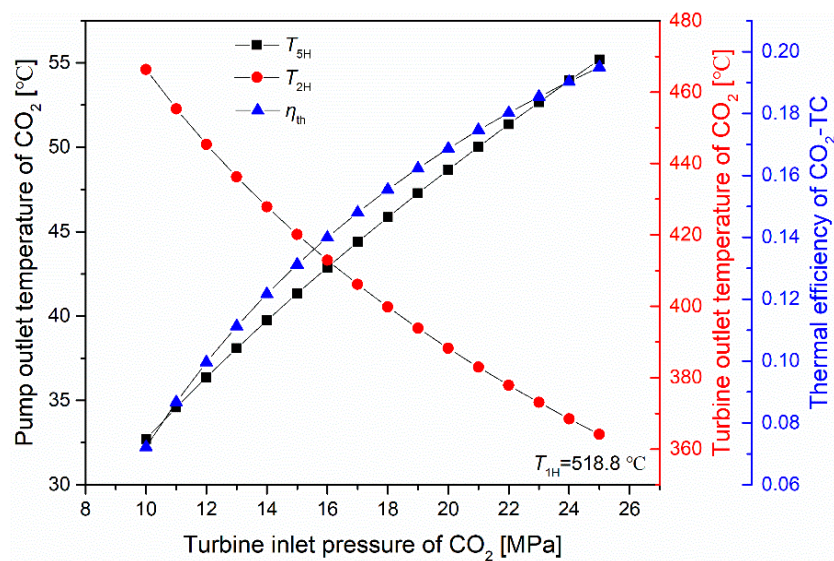


Figure 10. Variations of pump and turbine outlet temperatures and thermal efficiency with turbine inlet pressure of CO₂ for CO₂-TC.

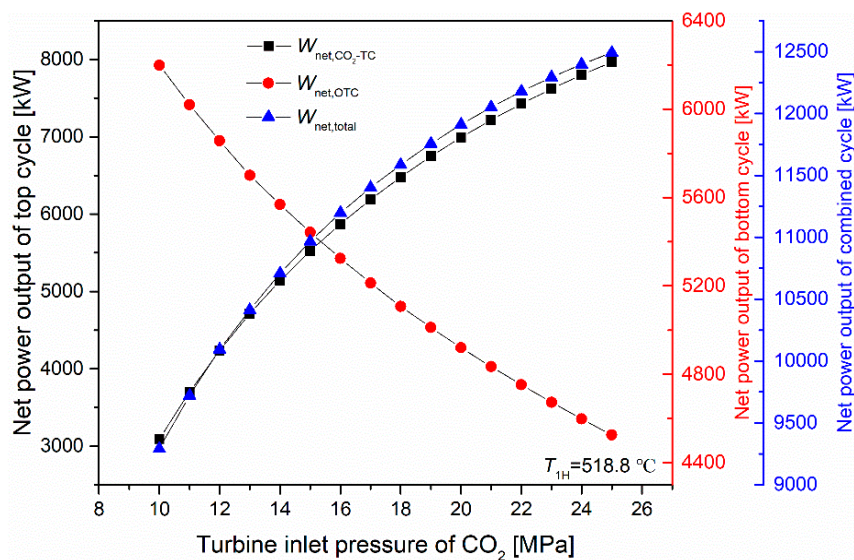


Figure 11. Variations of net power output with turbine inlet pressure of CO₂ for CO₂-TC/OTC.

The influence of the turbine inlet temperature of CO₂ (T_{1H}) on the system net power output is shown in Figure 12. The average heat absorption temperature and heat rejection temperature of CO₂-TC increase with the increase of T_{1H} , thus there exists an optimal T_{1H} to maximize the thermal efficiency and net power output of CO₂-TC since the heat input of the cycle remains unchanged. Although the mass flow rate of CO₂ decreases as T_{1H} increases, the maximum net power output of OTC still increases with the increase of T_{2H} . Finally, the maximum total net power output of the combined cycle CO₂-TC/OTC is obtained as T_{1H} reaches the upper limit.

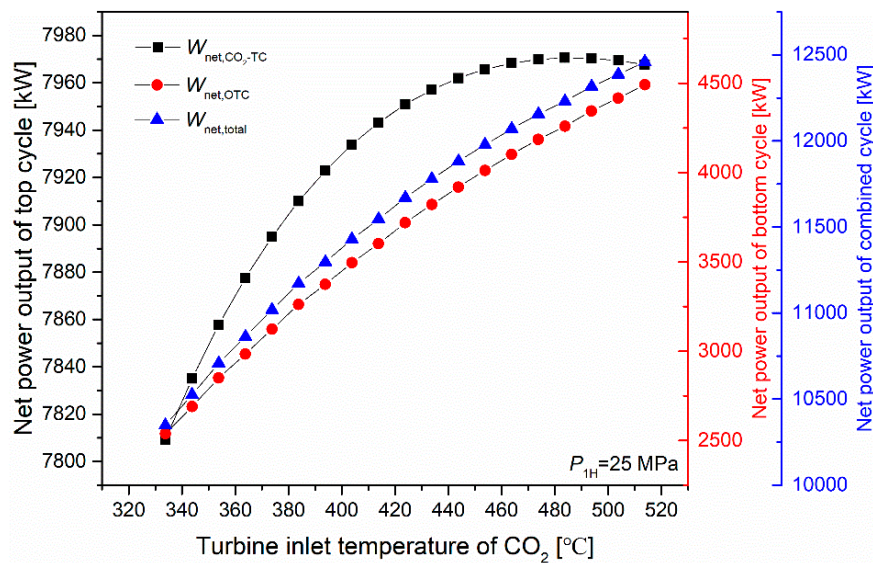


Figure 12. Variations of net power output with turbine inlet temperature of CO_2 for CO_2 -TC/OTC.

The optimized variables and the maximum net power output of combined cycle CO_2 -TC/OTC are listed in Table 5. Also, the optimal turbine inlet temperature and pressure of CO_2 are their respective upper limits for CO_2 -TC/OTC. Figure 13 shows the comparison of the net power output of two combined cycles and it can be seen that the net power output of CO_2 -TC+OTC is slightly higher than that of CO_2 -TC/OTC. The net power output of OTC in CO_2 -TC/OTC is higher than that of the OTC in CO_2 -TC+OTC and the pentane still outperforms R134a since it can extract a little more heat from the exhausted CO_2 with a lower thermal efficiency of the cycle, which have been revealed in the T-Q diagram of CO_2 and organic fluid in the IHE shown in Figure 14.

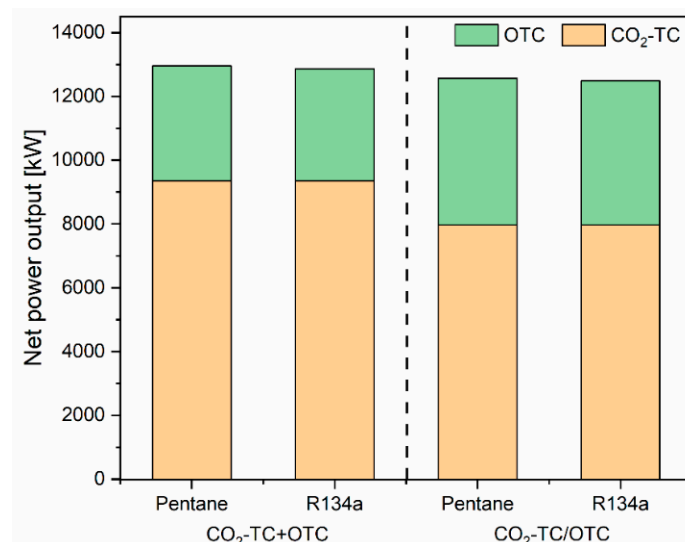


Figure 13. Net power output comparison of the two combined cycles.

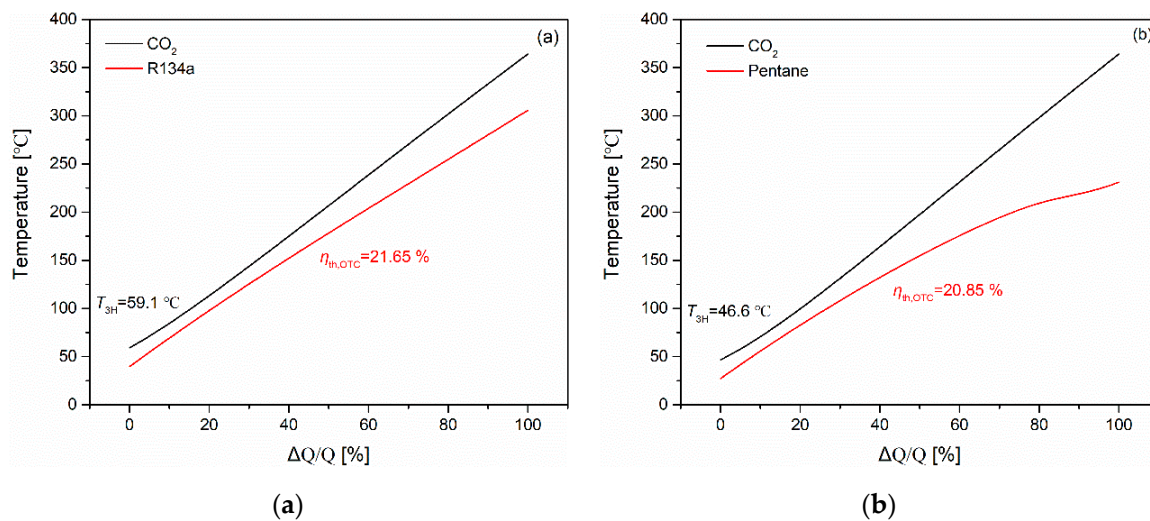


Figure 14. T-Q diagram of CO₂ and organic fluid (a) R134a, (b) Pentane in the intermediate heat exchanger (IHE) of CO₂-TC/OTC.

4.3. Exergy Analysis of the Two Combined Cycles

The exergy analysis to evaluate the exergy loss in each component of the two combined cycles is shown in Table 6. The input exergy of the cycle is equal to the net power output plus the total dissipated exergy in each component. For CO₂-TC+OTC, the sum of input exergy of top and bottom cycle and the exergy contained in the discharged gas is the total exergy of the heat source. For CO₂-TC/OTC, the input exergy of OTC is from the exhausted CO₂ and the heat source exergy is equal to the sum of the input exergy of the top cycle and the discharged gas exergy.

Table 6. The exergy inputs, outputs and losses for the combined cycles.

		CO ₂ -TC+OTC		CO ₂ -TC/OTC		
		R134a	Pentane	R134a	Pentane	
Top cycle	Exergy input (kW)	13,605.3	13,605.3	18,786.3	18,786.3	
	Power output (kW)	9353.9	9353.9	7966.6	7966.6	
	Exergy loss (kW)	HRVG	287.9	287.9	1912.1	1912.1
		Turbine	572.7	572.7	499.8	499.8
		recuperator	2400.2	2400.2	-	-
		condenser	617.8	617.8	401.6	280.5
	pump	372.8	372.8	318.3	318.3	
Bottom cycle	Exergy input (kW)	5371.4	5399.8	7687.7	7809	
	Power output (kW)	3511.4	3601.2	4523.3	4607.8	
	Exergy loss (kW)	HRVG/IHE	577.9	651.5	835.6	1507.4
		Turbine	519.6	635.5	613.5	637.5
		condenser	577.6	458.5	1472.9	999.9
		pump	184.9	53.1	242.2	56.4
Discharged gas	Exergy loss (kW)	150.1	121.7	340.5	340.5	
	Exergy efficiency of combined cycle (%)	67.26	67.73	65.30	65.74	

The exergy efficiency of CO₂-TC+OTC is about 2% higher than that of CO₂-TC/OTC. The distribution of the exergy loss in each component for the two combined cycles using pentane is shown in Figure 15. In CO₂-TC+OTC, the recuperation process causes the largest exergy loss, which is due to the large difference in specific heat capacity of the hot and cold fluids in the recuperator (see Figure 1). Recompression can effectively reduce the exergy loss in the recuperator and the $T_{g,m}$ will increase accordingly, which may lead to an increase of exergy loss in the organic HRVG. In CO₂-TC/OTC, the largest exergy loss occurs in HRVG, followed by IHE. The specific heat capacity of CO₂ and organic

fluid in the heat addition process changes markedly (see Figure 16), resulting in the poor thermal match between exhaust gas and CO₂ in HRVG and between CO₂ and organic fluid in IHE.

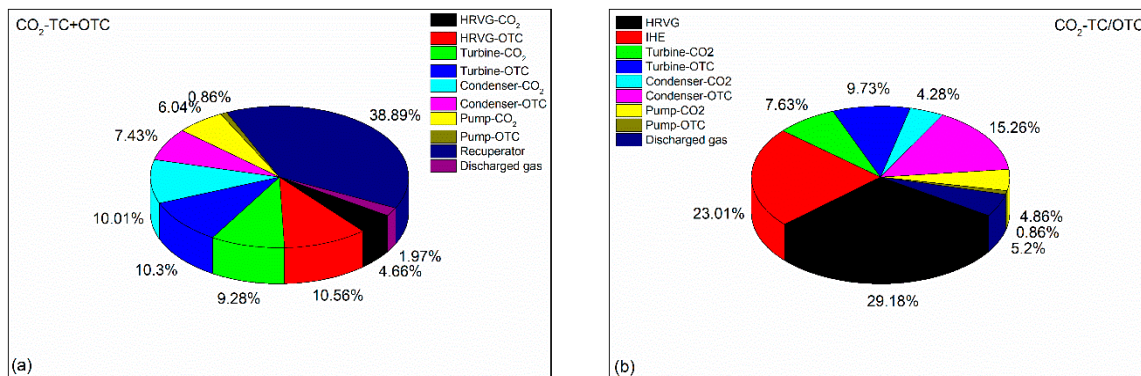


Figure 15. Distribution of exergy loss in each component of the combined cycle (a) CO₂-TC+OTC; (b) CO₂-TC/OTC.

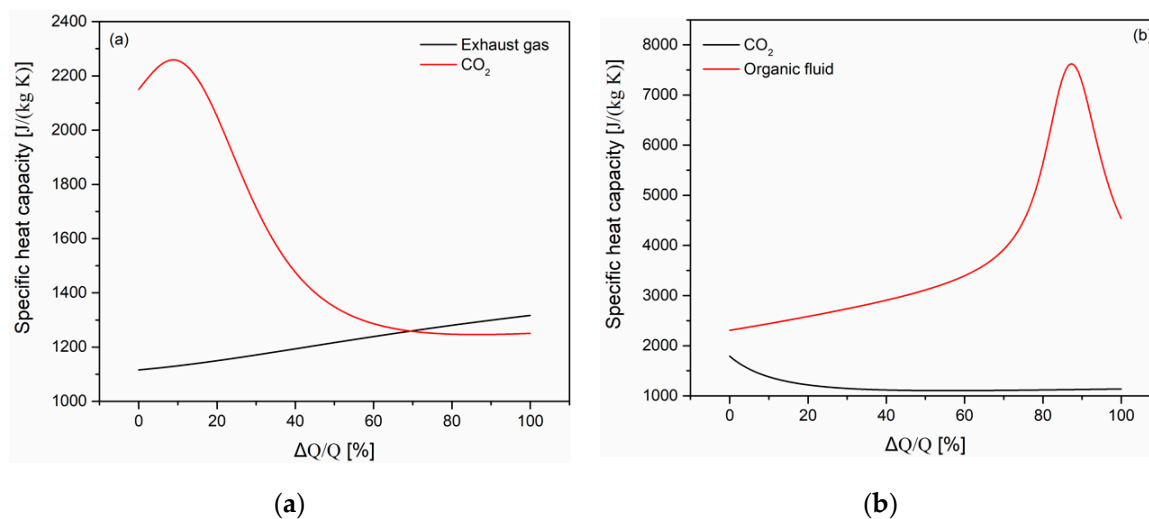


Figure 16. Variation of specific heat capacity of fluids in (a) HRVG; (b) IHE for CO₂-TC/OTC.

5. Conclusions

This study aims to compare the thermodynamic performance of two combined cycles that is, CO₂-TC+OTC and CO₂-TC/OTC, for waste heat recovery. Parameters optimization is performed by means of genetic algorithm to maximize the net power output of the cycle and exergy analysis is also examined to evaluate the exergy loss in each component. R134a and pentane are considered as the working fluid for the bottom OTC and the decision variables are turbine inlet temperature and pressure of CO₂ and organic fluid in the top and bottom cycle respectively. The main conclusions are briefly summarized below:

- (1) As the turbine inlet temperature and pressure of CO₂ increase, the total net power output of the combined cycle is increased, even though the net power output of the top or bottom cycle may decrease as a result.
- (2) The exergy efficiency of CO₂-TC+OTC is about 2% higher than that of CO₂-TC/OTC and pentane outperforms R134a in using as the working fluid for bottom OTC.
- (3) In CO₂-TC+OTC, the recuperation process of CO₂ causes the largest exergy loss due to the large difference in specific heat capacity of the hot and cold fluids in the recuperator. In CO₂-TC/OTC, the largest exergy loss occurs in HRVG, followed by IHE, which is attributed to the poor

temperature match in the heat exchanger caused by the larger variation of specific heat capacity of CO₂ and organic fluid in the heat addition process.

Author Contributions: Conceptualization, H.W.; Data curation, L.R.; Formal analysis, L.R.; Funding acquisition, H.W.; Investigation, L.R.; Methodology, L.R.; Project administration, H.W.; Software, L.R.; Writing—original draft, L.R.; Writing—review & editing, H.W. All authors have read and agreed to the published version of the manuscript.

Funding: This research was funded by the National Natural Science Foundation of China (No. 51376134).

Conflicts of Interest: The authors declare no conflict of interest.

Nomenclature

e	exergy (kJ/kg)
h	enthalpy (kJ/kg)
\dot{i}	exergy loss (kW)
\dot{m}	mass flow rate (kg/s)
P	pressure (kPa)
\dot{Q}	heat transfer rate (kW)
s	entropy (kJ/(kgK))
SP	size parameter (m)
T	temperature (°C)
V_r	volume ratio
\dot{W}	power (kW)

Greek Letters

η	efficiency
Δ	difference

Subscript

$crit$	critical
g	gas
in	inlet
m	medium
out	outlet
pp	pinch point
th	thermal
$turb$	turbine
wf	working fluid

Abbreviations

HRVG	heat recovery vapor generator
LCOE	Levelized cost of energy
OTC	organic trans-critical cycle
TC	trans-critical cycle
SC	supercritical cycle

References

- Chen, H.; Goswami, D.Y.; Stefanakos, E.K. A review of thermodynamic cycles and working fluids for the conversion of low-grade heat. *Renew. Sustain. Energy Rev.* **2010**, *14*, 3059–3067. [[CrossRef](#)]
- Pan, L.; Li, B.; Shi, W.; Wei, X. Optimization of the self-condensing CO₂ transcritical power cycle using solar thermal energy. *Appl. Eng.* **2019**, *253*, 113608. [[CrossRef](#)]
- Persichilli, M.; Kaculdis, A.; Zdankiewicz, E.; Held, T. Supercritical CO₂ Power Cycle Developments and Commercialization: Why sCO₂ can Displace Steam. In Proceedings of the Power-Gen India & Central Asia, Pragati Maidan, New Delhi, India, 19–21 April 2012.

4. Ahn, Y.H.; Bae, S.J.; Kim, M.S.; Cho, S.K.; Baik, S.J.; Lee, J.I.; Cha, J.E. Cycle layout studies of S-CO₂ cycle for the next generation nuclear system application. In Proceedings of the Korean Nuclear Society Autumn Meeting, PyeongChang, Korea, 30–31 October 2014.
5. Ahn, Y.; Lee, J.I. Study of various Brayton cycle designs for small modular sodium-cooled fast reactor. *Nucl. Eng. Des.* **2014**, *276*, 128–141. [[CrossRef](#)]
6. Zhang, Y.; Li, H.; Han, W.; Bai, W.; Yang, Y.; Yao, M.; Wang, Y. Improved design of supercritical CO₂ Brayton cycle for coal-fired power plant. *Energy* **2018**, *155*, 1–14. [[CrossRef](#)]
7. Binotti, M.; Astolfi, M.; Campanari, S.; Manzolini, G.; Silva, P. Preliminary assessment of sCO₂ cycles for power generation in CSP solar tower plants. *Appl. Eng.* **2017**, *204*, 1007–1017. [[CrossRef](#)]
8. Hou, S.; Wu, Y.; Zhou, Y.; Yu, L. Performance analysis of the combined supercritical CO₂ recompression and recuperated cycle used in waste heat recovery of marine gas turbine. *Energy Convers. Manag.* **2017**, *151*, 73–85. [[CrossRef](#)]
9. Cao, Y.; Ren, J.; Sang, Y.; Dai, Y. Thermodynamic analysis and optimization of a gas turbine and cascade CO₂ combined cycle. *Energy Convers. Manag.* **2017**, *144*, 193–204. [[CrossRef](#)]
10. Hou, S.; Zhou, Y.; Yu, L.; Zhang, F.; Cao, S. Optimization of the combined supercritical CO₂ cycle and organic Rankine cycle using zeotropic mixtures for gas turbine waste heat recovery. *Energy Convers. Manag.* **2018**, *160*, 313–325. [[CrossRef](#)]
11. Astolfi, M.; Alfani, D.; Lasala, S.; Macchi, E. Comparison between ORC and CO₂ power systems for the exploitation of low-medium temperature heat sources. *Energy* **2018**, *161*, 1250–1261. [[CrossRef](#)]
12. Wright, S.A.; Davidson, C.S.; Scammell, W.O. Thermo-economic analysis of four sCO₂ waste heat recovery power systems. In Proceedings of the 5th International Symposium on Supercritical CO₂ Power Cycles, San Antonio, TX, USA, 29–31 March 2016.
13. Akbari, A.D.; Mahmoudi, S.M. Thermo-economic analysis & optimization of the combined supercritical CO₂ (carbon dioxide) recompression Brayton/organic Rankine cycle. *Energy* **2014**, *78*, 501–512.
14. Li, C.; Wang, H. Power cycles for waste heat recovery from medium to high temperature flue gas sources—from a view of thermodynamic optimization. *Appl. Eng.* **2016**, *180*, 707–721. [[CrossRef](#)]
15. Manente, G.; Fortuna, F.M. Supercritical CO₂ power cycles for waste heat recovery: A systematic comparison between traditional and novel layouts with dual expansion. *Energy Convers. Manag.* **2019**, *197*, 111777. [[CrossRef](#)]
16. Ren, L.; Wang, H. Parametric optimization and thermodynamic performance comparison of organic trans-critical cycle, steam flash cycle, and steam dual-pressure cycle for waste heat recovery. *Energies* **2019**, *12*, 4623. [[CrossRef](#)]
17. Lemmon, E.W.; Huber, M.L.; McLinden, M.O. *Reference Fluid Thermodynamic and Transport Properties REFPROP*; Version 9.0; National Institute of Standards and Technology: Gaithersburg, MD, USA, 2013.
18. Haglind, F.; Elmegaard, B. Methodologies for predicting the part-load performance of aero-derivative gas turbines. *Energy* **2009**, *34*, 1484–1492. [[CrossRef](#)]
19. Macchi, E.; Astolfi, M. *Organic Rankine Cycle (ORC) Power Systems—Axial Flow Turbines for Organic Rankine Cycle Applications*; Woodhead Publishing, Politecnico di Milano: Milan, Italy, 2017; Volume 9, pp. 299–319.
20. Dai, X.; Shi, L.; An, Q.; Qian, W. Chemical kinetics method for evaluating the thermal stability of Organic Rankine Cycle working fluids. *Appl. Therm. Eng.* **2016**, *100*, 708–713. [[CrossRef](#)]
21. Calderazzi, L.; di Paliano, P.C. Thermal stability of R-134a, R-141b, R-1311, R-7146, R-125 associated with stainless steel as a containing material. *Int. J. Refrig.* **1997**, *20*, 381–389. [[CrossRef](#)]

